Title

Mechanical strength and electrical conductivity of Cu-In solid solution alloy wires

Author(s)

Yasunori Abe, Satoshi Semboshi, Naoya Masahashi, Sung Hwan Lim, Eun-Ae Choi, Seung Zeon Han

Journal

Metallurgical and Materials Transactions A 54, 928–938

Published

28 December 2022

URL（The Version of Record）

https://doi.org/10.1007/s11661-022-06938-1

Mechanical strength and electrical conductivity of Cu-In solid solution alloy wires

Yasunori Abe[a], Satoshi Semboshi[a,*], Naoya Masahashi[a], Sung Hwan Lim[b], Eun-Ae Choi[c], Seung Zeon Han[c]

[a] Institute for Materials Research, Tohoku University, Katahira 2-1-1, Aoba-ku, Sendai, Miyagi 980-8577 h, Japan, JPN

[b] Department of Advanced Materials Science & Engineering, Kangwon National University, Chuncheon 200-701, Republic of Korea, KOR

[c] Korea Institute of Materials Science, 797 Changwondaero, Seongsan-gu, Changwon, Gyeongnam 51508, Republic of Korea, KOR

Corresponding author (S. Semboshi) E-mail: satoshi.semboshi.c8@tohoku.ac.jp, Tel: +81-22-215-2220, FAX: +81-22-215-2220

Y. Abe: abeyasu326@gmail.com

S. Semboshi: satoshi.semboshi.c8@tohoku.ac.jp

N. Masahashi: masahasi@imr.tohoku.ac.jp

E.A. Choi: eunae.choi@kims.re.kr

S.H. Lim: shlim@kangwon.ac.kr

S.Z. Han: szhan@kims.re.kr

Abstract

Conductive spring wires for application in electrical components require high strength, high electrical conductivity, and convenient manufacturability. Copper-indium (Cu-In) solid solution alloys are suitable candidates for such wires because they exhibit effective solid solution strengthening without significantly decreasing the conductivity. Herein, we systematically investigate the microstructure of Cu-In alloy wires fabricated by severe drawing, along with their mechanical and electrical properties. During the initial drawing stages, high-density deformation twins are generated in the Cu-In alloy because the In solute efficiently reduces the stacking fault energy (SFE) of the Cu matrix. These deformation twins promote grain refinement during

subsequent drawing. The Cu-5.0 at.% In alloy wire, drawn severely to an equivalent strain of 4.61, possesses ultrafine grains measuring 60–80 nm with a high density of dislocations, resulting in excellent yield strength, tensile strength, and conductivity of 1280 MPa, 1340 MPa, and 24% relative to the International Annealing Cu Standard, respectively. These properties were comparable to those of age-hardenable Cu-Be and Cu-Ti alloys; thus, our results demonstrate that tuning the In content of the Cu matrix to reduce the SFE and optimizing the deformation strain to refine the grain size significantly improves the performance of alloy wires.

Keywords: Cu-In alloys; severe plastic deformation (SPD); grain refinement; strengthening; electrical conductivity; stacking fault energy (SFE)

---

1. Introduction

Recent innovations in electronic devices and products have revealed a need to enhance the mechanical strength and electrical conductivity of Cu-based alloy wires and sheets used in electrical components, connective wires and springs, connectors, and lead frames. Over several decades, numerous studies have sought to control the microstructure to tailor the properties of various types of Cu alloys to suit diverse applications. The conventional Cu-based alloys used in such wires and sheets are classified into two types: solid solution strengthened and age-hardenable alloys. Solid solution strengthened alloys (e.g., Cu-Sn, Cu-Zn, and Cu-Ni) are made by a simple manufacturing process that consumes less energy than that used in the fabrication of age-hardenable alloys (e.g., Cu-Be, Cu-Ni-Si, and Cu-Ti) which requires supersaturated solid solution and then aging heat-treatments [1–5]. However, solid solution strengthened alloys require large amounts of solutes to improve their strength, which inevitably reduces their conductivity [6,7]. Thus, realizing a simultaneous improvement in the strength and conductivity of solid solution strengthened Cu alloys is more difficult than in age-hardenable alloys. The production of solid solution strengthened alloys exhibiting a combination of mechanical strength and electrical conductivity comparable to those of age-hardenable alloys for use in electrical applications is therefore of great importance.

The design of solid solution strengthened Cu alloys typically includes a solute element that contributes to strengthening without significantly reducing conductivity. In addition, solid solution strengthening can be effectively combined with other strengthening mechanisms through deformation strain and grain refinement by severe plastic deformation (SPD) processing [8,9], which is particularly applicable to the production of thin wires and sheets. SPD processing does not significantly reduce the conductivity of the material because structural defects, such as dislocations and grain boundaries, have a less significant effect on the conductivity and resistivity [10–12]. SPD processing typically employs low alloying solid solution Cu alloys to fabricate products owing to their ductility, which prevents fracturing during plastic deformation. Notably, the grain refinement resulting from the formation of deformation twins is effectively induced during SPD processing if the solute element reduces the stacking fault energy (SFE). For example, a Cu-30 at.% Zn alloy processed by high-pressure torsion exhibited an average grain size of only 10 nm, with a remarkably low SFE of 7 mJ/m^2 [13,14]. The microstructural evolution during SPD also led to favorable mechanical properties such as enhanced yield strength and toughness in low-SFE Cu-Al and Cu-Zn alloys with face-centered cubic (fcc) metals [14–17].

Given this context, highly strengthened and highly conductive Cu alloy thin sheets and wires may be obtained from Cu-In solid solution alloys: the rate at which the conductivity declines with an increasing amount of dissolved In in the Cu matrix is lower than that observed with other elements such as Al, Ni, and Sn [6,19]. Effective solid solution strengthening is expected when In atoms are dissolved in the Cu matrix owing to the large atomic size effect of Cu [20], however, solid solution strengthening in Cu-In alloys has not been reported. Gallagher reported that a Cu-3.2

at.% In alloy showed an SFE of approximately 29 mJ/m^2 [21]. This suggests that the SFE of pure Cu (~78 mJ/m^2 [21–25]) is significantly reduced by the addition of In. The observed SFE is comparable to that of low-SFE Cu-5 at.% Al alloy, (25–28 mJ/m^2 [24,25]), and significantly lower than that of Cu-5 at.% Zn: (53 mJ/m^2 [22]). A significant strengthening in low-SFE Cu-In alloy wires and sheets is therefore expected owing to effective grain refinement by the generation of high-density deformation twins during SPD processing.

In this study, we fabricated Cu-In alloy wires with a suitable combination of high mechanical strength and electrical conductivity via severe drawing. We confirmed the compositional dependence of the microstructure, electrical conductivity, and mechanical properties of Cu-In solid solution alloys. We then optimized the composition of the Cu-In alloy and demonstrated the fabrication of high-performance Cu-In alloy wires by severe drawing. Finally, we measured the microstructural evolution and its effect on the mechanical and electrical properties of the alloy during severe drawing. We also propose a mechanism for the strengthening of the Cu-In alloy wires based on our observations.

2. Materials and methods

Pure Cu and five Cu-In solid solution alloys with In contents of 1.0, 2.5, 4.0, 5.0, and 7.5 at.% were used to examine the compositional dependence of the microstructure and properties on the In content. The alloys were prepared from melting Cu tips (99.99%) and indium grains (99.99%) using a high-frequency induction-heating apparatus in an argon atmosphere, followed by casting into a Cu mold to obtain bullet-shaped ingots measuring 15 mm in diameter and 70 mm in length. According to the phase diagram of the Cu-In system, the solubility limit of In in Cu solvent at 700 °C was approximately 10 at.% [26]. Based on the phase diagram, the Cu-(0 to 7.5) at.% In alloy ingots were heat-treated at 700 °C for 72 h in air and subsequently quenched in water to obtain a single-phase Cu solid solution (Cu_{ss}) without segregation. The contaminated layer on the ingot surface was removed by mechanical machining to obtain cylindrical ingots of a diameter 12 mm. The cylindrical Cu-(0 to 5.0) at.% In alloy ingots were deformed into rods measuring 3.0 mm in diameter and over 600 mm in length via hot forging at 700 °C and cold-groove rolling, although the cylindrical Cu-7.5 at.% In alloy ingot was fractured during cold-groove rolling. The rods of Cu-(0 to 5.0) at.% In alloys were heat-treated within a single-phase region of Cu_{ss} at 500 °C for 1 min and then immediately quenched in water to remove the deformation strain during previous cold-groove rolling. The contaminated surface of the rods was polished using 600-grade emery paper, and the rods were subsequently drawn to wires at 20 °C with a reduction ratio of less than 0.20 in equivalent strain (ε) per drawing pass. The rods were then drawn to ε = 6.80 (i.e., the diameter of the rods was reduced from 3.0 mm to 0.1 mm) at maximum. Here, the ε during drawing is defined as $\varepsilon = 2\ \ln(d_o/d)$, where d_o and d represent the diameters of the rods and wires before and after drawing, respectively.

X-ray diffraction (XRD) was performed using a PANalytical X'Pert Pro diffractometer with CuK_α radiation at 40 kV to reveal the structure of the Cu-In alloys. Here, the cylindrical specimens with a single phase of Cu_{ss} were subjected to XRD measurements because it required a specimen with a large cross-section. The cross-sectional microstructures of the Cu-In alloy rods and wires were observed using field-emission scanning electron microscopy (FE-SEM, JEOL JSM–7001F) combined with electron backscatter diffraction (EBSD) at a voltage of 15 kV. Before the FESEM-EBSD analysis, the rods and wires were fixed in resin, mechanically polished using a fine Al_2O_3 slurry, and finished by ion milling (HITACHI IM4000PLUS). In the EBSD analysis, each pair of points with a misorientation angle in excess of 15° (except for isolated pixels and noise from dirt on the surface) was considered a grain boundary (GB) for statistical purposes (low-angle GBs with a crystal orientation difference of less than 15° are not presented). Further, the microstructure of the samples was observed using transmission electron microscopy (TEM, JEOL JEM-2000EXII) operated at an accelerating voltage of 200 keV. Thin-foil specimens for TEM observation were mechanically polished to a thickness of less than 30 μm and subjected to low-angle ion milling (JEOL PIPS) with acceleration voltages of less than 3.0 keV using high-purity argon gas.

The electrical conductivity of the 12 mm-diameter cylindrical ingots was measured using an Eddy current conductivity measuring method and that of the rods and wires was measured by a constant 10 mA direct-current four-probe method at 20 °C. The Vickers hardness of the rods and wires was measured using a Mitsutoyo HM-101 Micro Vickers Hardness Testing Machine with an applied load of 1.96 N for 10 s; the hardness values are quoted as the average of 10 indentations. The rods and wires were fixed using resin and mechanically ground to obtain the flat surface required for the hardness measurements. Tensile tests were performed on the wires at 20 °C at an initial strain rate of 1.67×10^{-4} s^{-1} using an Autograph AG-IS (Shimadzu). The yield strength (0.2% proof stress) and ultimate tensile strength were obtained by averaging at least three measurements. The Young's modulus of the straight rods with a diameter and length of 3.0 and 50 mm, respectively, was measured via the free resonance vibration method using NihonTehno-Pluse JE-LHT.

3. Results

3.1 Fundamentals of Cu-In solid solution alloys

3.1.1 Microstructure

Figure 1 shows the inverse pole figure (IPF) maps obtained via EBSD analysis of the transversal cross-section of the pure Cu and Cu-1.0, 2.5, 4.0, and 5.0 at.% In alloy rods, which were heat-treated at 500 ^{o}C and then quenched. This reveals that all Cu-In alloy specimens consisted of a single phase of typical equiaxial Cu_{ss} grains by recovery and recrystallization. The average grain size of the pure Cu rod was approximately 22 μm, while it decreased to less than 10 μm in the Cu-In alloy rods.

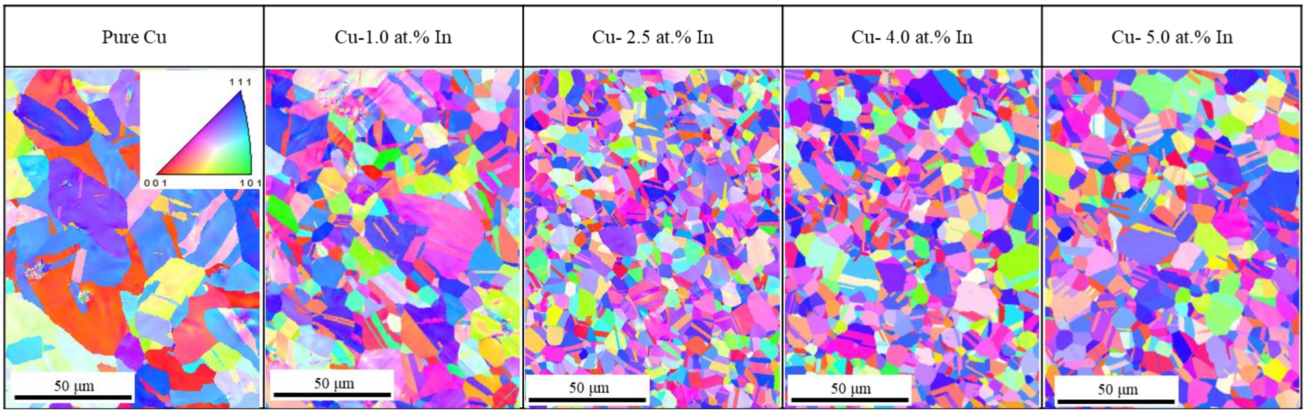

Fig. 1 Inverse pole figure (IPF) obtained by EBSD of the cross-section of the pure Cu and Cu-1.0, 2.5, 4.0, and 5.0 at.% In alloy rods.

Figure 2 compares the variation of the lattice parameter of Cu-In alloys, as a function of In content, with that of conventional Cu_{ss} alloys, which were determined by extrapolating the values obtained from the XRD profiles using the Nelson-Riley function [27]. Here, the cylindrical alloy ingots, which were heat-treated at 700 °C and then quenched, were subjected to XRD measurements, because they have a sufficiently large cross-section to obtain the XRD profile. Note that the all the Cu-(1.0 to 7.5) at.% In alloy cylindrical ingots have a single phase of Cu_{ss}, as confirmed by XRD measurement and FE-SEM images. The lattice parameter of the Cu_{ss} phase increased linearly with the In content of the alloy, which follows Vegard's relationship:

$$a\ [\mathrm{nm}] = 0.3615 + 0.00097\ C_{\mathrm{In}}, \quad (1)$$

where a represents the lattice parameter of the Cu-In alloy. The gradient of Vegard's relationship for Cu-In alloys is greater than that of most other conventional Cu_{ss} alloys except the Cu-Sn alloy [28].

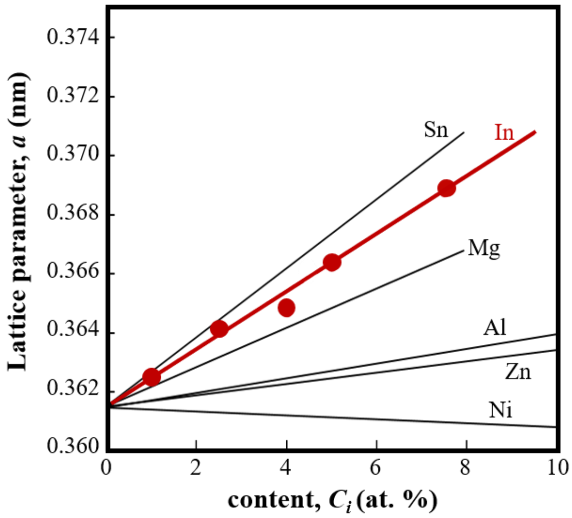

Fig. 2 Comparison of the lattice parameters of Cu-In solid solution alloys with other Cu solid solution binary alloys (Cu-Sn, Cu-Mg, Cu-Al, Cu-Zn, and Cu-Ni [28]). The lattice parameter of the Cu solid solution alloys increases essentially linearly with the solute content.

3.1.2 Electrical conductivity and resistivity

Figure 3 shows the electrical conductivity and resistivity of the Cu-In alloy ingots with a single phase of Cu_{ss}, which were quenched from 700 °C. The electrical conductivity of the Cu-In alloy, σ^e, decreased with increasing In content. This means that the electrical resistivity of the Cu-In alloy, ρ^e, increased with increasing In content. The liner increase in ρ^e shown in Fig. 3 can be explained by Nordheim's equation, which relates the concentration of the In solute to the resistivity, and is given as follows:

$$\rho^e = \rho^e_{\mathrm{Cu}} + A\, C_i\, (100 - C_i), \tag{2}$$

where ρ^e_{Cu}, C_i (at.%), and A (Ω m/at.%) are the resistivity of pure Cu (1.724×10^{-8} Ω m at 20 °C), atomic composition of the solute element, and relative resistivity, respectively, the latter of which depends on the solute species and the host metal. In the Cu-In alloys with an In content of 0–7.5 at.%, A could be fit as 0.83×10^{-8} Ω m/at.% In (Fig. 3). This value is relatively small compared to that of other conventional solute elements in Cu, as shown in Table 1 [6,19, 29–32]. This is consistent with Linde's rule [19], which states that elements closer to Cu in the periodic table tend not to significantly reduce the resistivity when alloyed with Cu.

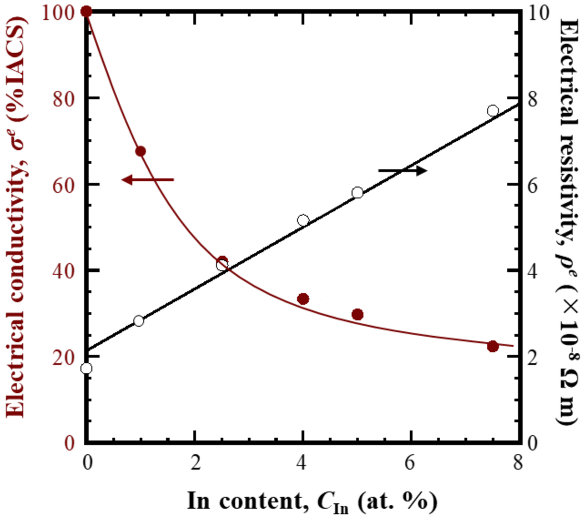

Fig. 3 Electrical resistivity and conductivity of Cu-In solid solution alloys, which were measured using an Eddy current conductivity method. The electrical conductivity is presented by the percentage of international annealed copper standard (% IACS) at 20°C of 5.8×10^7 / Ω m. The electrical resistivity of the alloys (open circle) increases linearly with the In content. (It increases parabolically with the In content, which follows Nordheim's equation, Eq. (2)). The electrical conductivity of the alloy (closed circle) is the inverse of the electrical resistivity.

Table 1 Increase rate depending on solid solution element to electrical resistivity of pure copper [6,19,29–32].

Element	*A* [10^{-8} Ωm/at%]	Element	*A* [10^{-8} Ωm/at%]
Zn	0.32	Sn	2.88
In	0.83	Cr	3.60
Al	1.23	Si	3.95
Ni	1.25	Ti	10.2

3.1.3 Mechanical properties

Figure 4 shows the average yield strength of the Cu–(0 to 5.0) at.% In alloy rods with a single fcc Cu_{ss} phase. The yield strength of Cu-5.0 at.% In alloy was approximately 140 MPa, which is greater than those of the Cu-5.0 at.% Al (~115 MPa) and Cu-5.0 at.% Ni (~60 MPa) alloys having a grain size similar to the Cu-5.0 at.% In alloy (approximately 10 μm) [33]. The yield strength of the

Cu-In alloys increases linearly with increasing $C_{In}^{2/3}$, demonstrating that the Cu-In alloys are strengthened by the solid solution of In atoms based on the Labusch theory [34,35]. The degree of solid solution strengthening by the In solute atoms in Cu_{ss} is related to the linear size factor (LSF), which represents the relative difference in the atomic size of the solute and solvent in a solid solution alloy; the LSF of In atoms for Cu is approximately 21.4%, which is higher than those of other elements typically alloyed with Cu, e.g., 5.4% for Zn, 6.3% for Al, 2.9% for Ni, 1.7% for Si, and 7.9% for Ti, but is lower than the 22.4% for Sn [20,29]. This result is consistent with the observed variations in the lattice parameters (Fig. 2). Therefore, solid solution strengthening by In in the Cu matrix is expected to be more effective than that achieved by other elements in conventional Cu alloys.

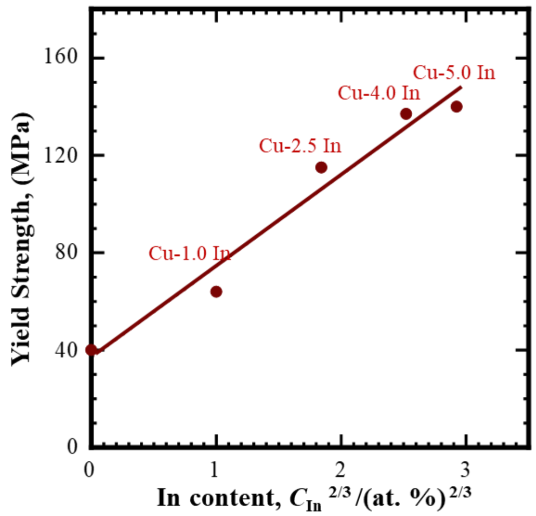

Fig. 4 Average yield strength of Cu-In solid solution alloys plotted as a function of $C_{In}^{2/3}$.

Figure 5 shows Young's moduli of various Cu–(0 to 5.0) at.% In alloy rods with a single Cu_{ss} phase. Young's modulus of pure Cu is 139 GPa, which is in approximate agreement with the reported value of 120–135 GPa [36,37]. Young's modulus decreased as the In content in the Cu-In alloys increased. The decreasing ratio of Young's modulus was estimated to be 3.9 GPa/at.% In. The reduction in Young's modulus may explain the fact that the melting point of the single Cu_{ss}

phase decreases significantly with an increase in the In content, as shown in the Cu-In phase diagram [26]. The alloy with a low melting point has a weak interatomic bond and large interatomic distance, resulting in a low Young's modulus.

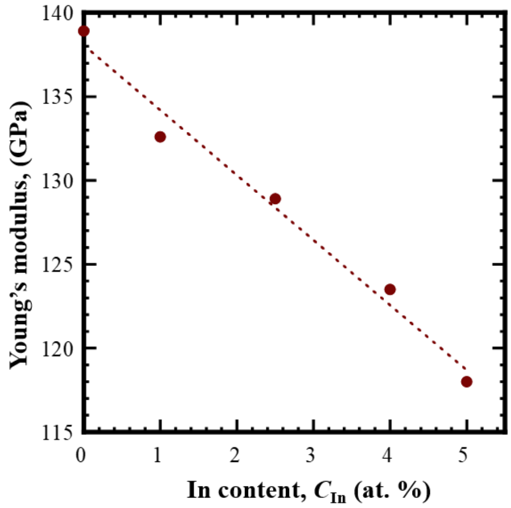

Fig. 5 Young's moduli of Cu-In solid solution alloys. The Young's moduli of the alloys decreased with increasing In content.

3.2. Microstructural evolution during drawing

A Cu-In alloy with high In content exhibits a low Young's modulus and high yield strength without any significant degradation in electrical conductivity. Such desirable characteristics of the Cu alloy enable its application as conductive spring wires, and therefore, we fabricated Cu-In solid solution alloy wires. Cu–0, 1.0, 2.5, 4.0, and 5.0 at.% In alloy rods with a diameter of 3.0 mm were successfully drawn down to less than 0.3 mm in diameter (i.e., more than an equivalent strain ε of 4.61) without any cracks and failure. Meanwhile, the Cu–7.5 at.% In alloy was fractured during cold-groove rolling before drawing, indicating insufficient plastic deformability. Accordingly, Cu-In alloys should be limited to a maximum In content of approximately 5.0 at.% to ensure that they can be significantly drawn without cracks and failure.

Figure 6 shows the GB distribution maps obtained via EBSD analysis of the transversal cross-section of the Cu-(0 to 5.0) at.% In alloy wires after drawing to ε = 0.81 (2.0 mm) and ε = 4.61 (0.3

mm). Before drawing, all Cu-(0 to 5.0) at.% In alloy rods contain typical equiaxial Cu_{ss} grains, as shown in Fig. 1. During the initial stage of drawing to ε = 0.81 (2.0 mm), deformation twin boundaries are formed in the parent grains, which increase in number with increasing In content (red lines in Fig. 6(a)). This was confirmed by measuring the fraction of the twin boundaries among the high-angle GBs with a misorientation > 15° (Figure 7). The fraction of twin boundaries in the Cu-5.0 at.% In alloy wire drawn to ε = 0.81 (2.0 mm) was 37%, which is significantly higher than that of both pure Cu and Cu-1.0 at.% In alloy wire (approximately 10%). This reveals that a higher number of deformation twins are generated while drawing Cu_{ss} alloys with a higher In content.

The grain size in the Cu-In alloy wires decreases during drawing (Figures 1 and 6). Particularly, in the case of the Cu-5.0 at.% In alloy wire drawn to ε = 4.61 (0.3 mm), it was difficult to obtain reliable EBSD results in some regions, due to insufficient grain size to detect clear Kikuchi patterns. The transverse-section TEM image of the Cu-5.0 at.% In alloy wire (Figure 8(a)) drawn to ε = 4.61 (0.3 mm) show fine grains containing modulated contrasts caused by the accumulated strain (dislocations). A sub-grain cell structure with nanotwin boundaries in the extended fibrous grains can be observed in the longitudinal cross-sectional TEM images (Figs. 8(b) and (c)). The grain size ranges from 60 to 80 nm in equivalent diameter as measured from the transverse and longitudinal cross-sectional TEM images.

The underlying mechanisms of the microstructure evolution, including grain refinement by SPD processing, can be categorized into two types: dislocation subdivision and deformation twin fragmentation [38,39]. In fcc metals with high or medium SFEs, such as pure Al (SFE γ: ~150 mJ/m^2) and Cu (~78 mJ/m^2), the majority of the plastic deformation is achieved via dislocation subdivision under less severe deformation conditions. However, the deformation and refinement of fcc metals with lower SFEs (e.g., high alloying solid solution Cu alloys of Cu–11.6 at.% Al (8 mJ/m^2) and Cu-30 at.% Zn (7 mJ/m^2)) under a more severe conditions is achieved primarily by the twin fragmentation mechanism [38,40]. The SFE of the Cu–5.0 at.% In alloy is expected to be significantly lower than that of the Cu–3.2 at.% In alloy (29 mJ/m^2) [21]. Therefore, it is rational to suggest that the deformation twin fragmentation mechanism was in operation during severe drawing to ε = 4.61 (0.3 mm), as per the following sequence: (i) Equiaxed grains are divided into deformation twins via partial dislocation emissions from the GBs owing to the low SFE of the Cu-5.0 at.% In alloy. In addition, the density of the deformation twins increases with increasing strain (Fig. 6(a), right). (ii) The increased strain is associated with an increase in deformation twins and dislocation accumulation. The accumulation of dislocations at the twin boundaries bends the original flat coherent twin boundaries. (iii) The larger deformation strain inevitably leads to the formation of sub-grains with both low-angle and high-angle GBs via the transformation of the coherent twin boundaries, thereby resulting in grain refinement with an average grain size of 60–80 nm (Fig. 8).

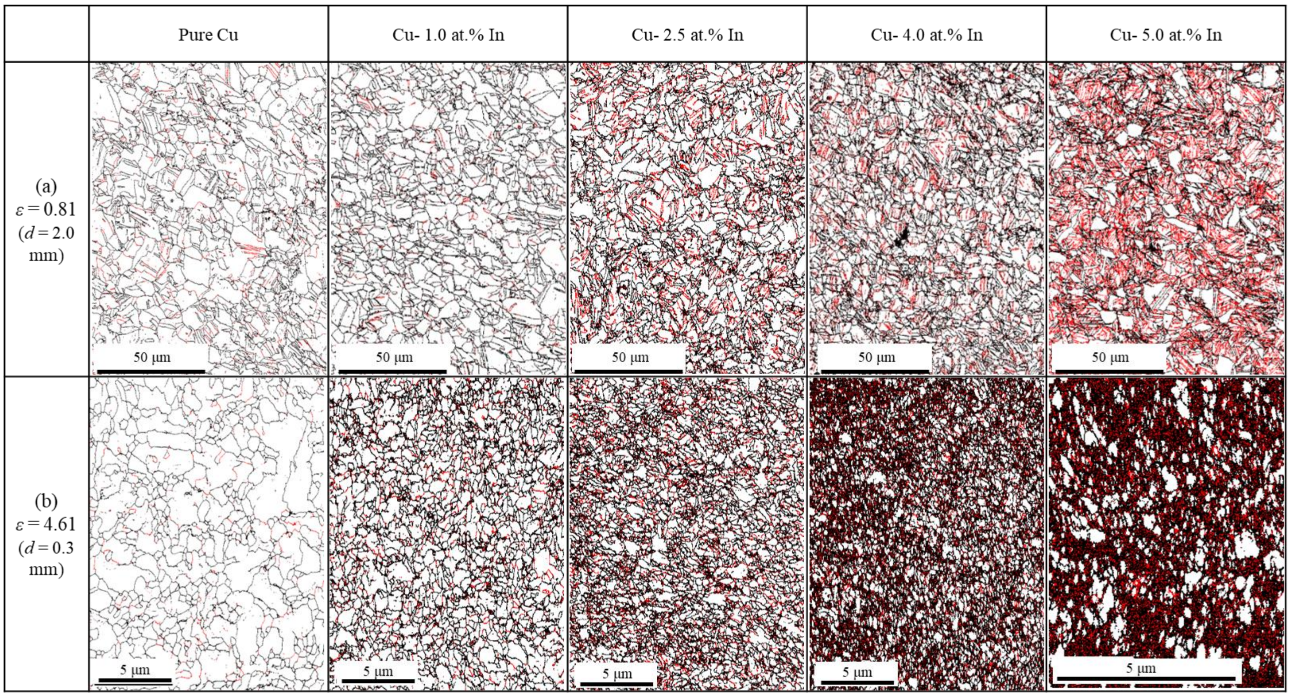

Fig. 6 Brain boundary (GB) maps obtained by EBSD of the cross-section of the Cu-(0 to 5.0) at.% In alloy wires drawn to (a) 2.0 mm (ε = 0.81), and (b) 0.3 mm (ε = 4.61), where high-angle GBs with an orientation angle in excess of 15° (random GBs) are depicted by solid back lines, while twin boundaries corresponding to a misorientation angle of 55–62.8° are indicated by red lines.

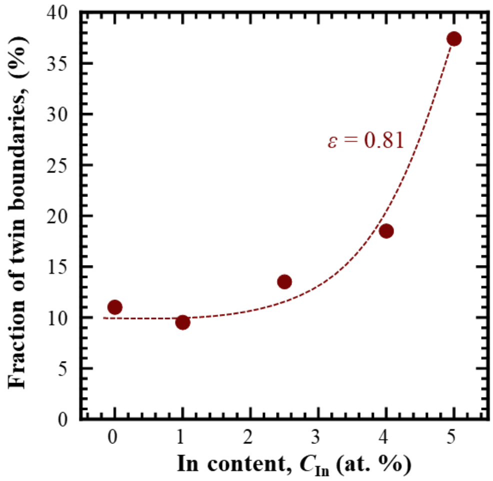

Fig. 7 Fraction of twin boundaries in high-angle GBs in Cu-In solid solution alloy wires drawn to ε = 0.81 (2.0 mm), as determined via EBSD.

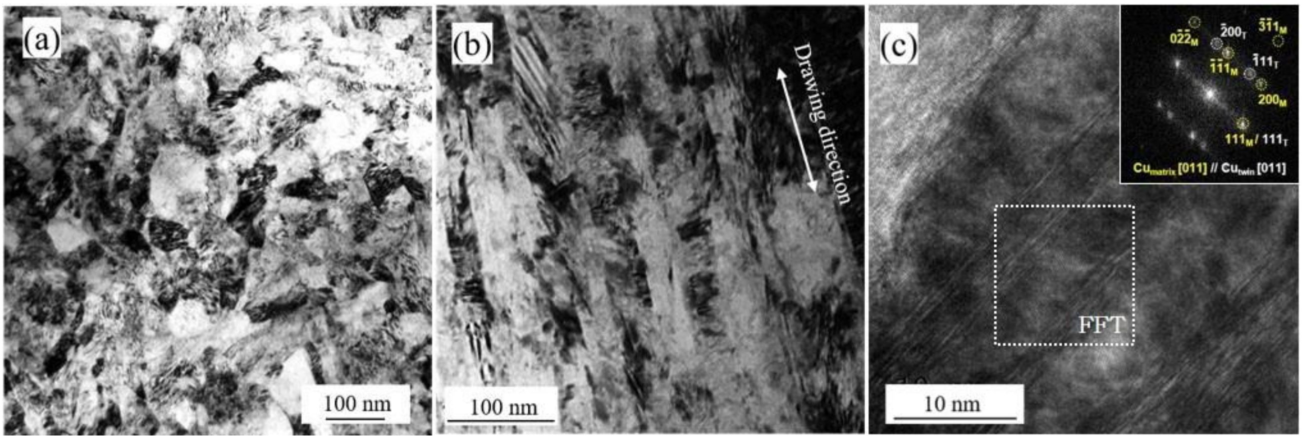

Fig. 8 (a) Transverse and (b), (c) longitudinal sectional bright-field TEM images, together with fast Fourier transform pattern captured from the dotted square in (c), of Cu–5.0 at.% In alloy wire drawn to ε = 4.61 (0.3 mm).

3.3. Properties of the drawn wire

3.3.1 Electrical conductivity and resistivity

Figure 9 shows the variations in the electrical conductivity and resistivity of the Cu-In alloy wires as a function of ε by drawing, together with those of pure Cu. The electrical resistivity of the Cu-In alloy rods before drawing increased with In content in accordance with Nordheim's equation (Fig.

3). The electrical conductivity (i.e. the reciprocal of the electrical resistivity) of all Cu-In alloys and pure Cu, decreased gradually with increasing ε. However, the reduction in the conductivity during drawing was less than 5% IACS even in the Cu-5.0 at.% In alloy wire drawn severely to ε = 4.61 (0.3 mm) (resistivity increase is only 1.0×10^{-8} Ω m). The reduction in electrical conductivity (i.e., increase in resistivity) after severe drawing can be explained by an increase in the number of structural defects, including dislocations and GBs arising from plastic deformation.

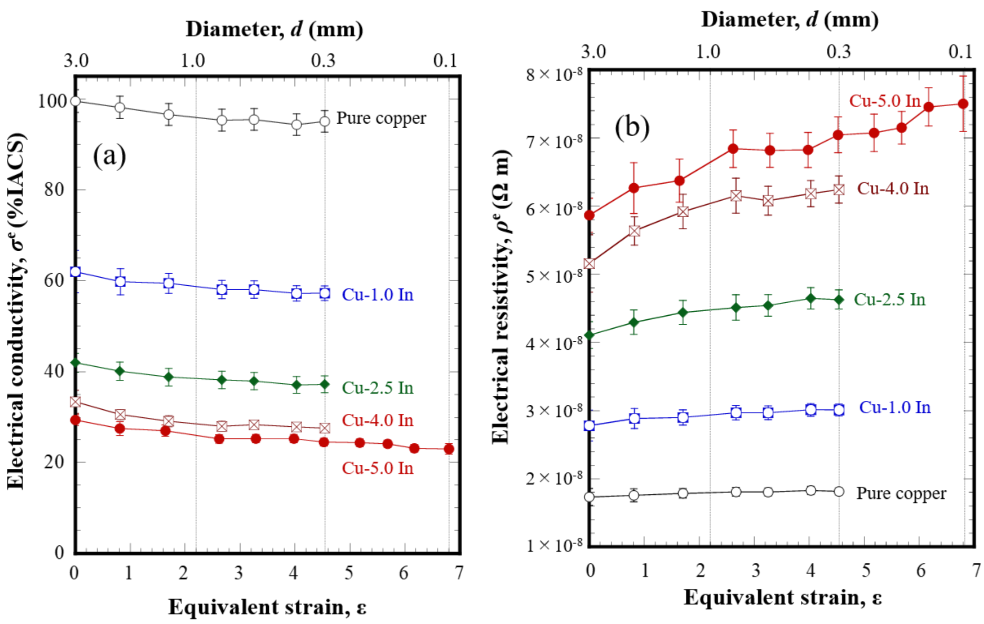

Fig. 9 Variations in electrical conductivity (a) and resistivity (b) of pure Cu and Cu-(1.0 , 2.5, 4.0, and 5.0) at.% In alloy wires as a function of an equivalent strain ε by drawing.

3.3.2 Mechanical properties

Figure 10 shows the Vickers hardness of the wires drawn from the Cu-In alloy rods as a function of ε by drawing, together with that of pure Cu. The Vickers hardness of the Cu-In alloy rods before drawing increased with the In content of the alloys, which is consistent with the trend displayed by the average yield strength (Fig. 4). The Vickers hardness of the drawn Cu-In alloy wires increased steadily with increasing ε; however, the hardness of the pure Cu wires only increased during the initial stage of drawing to ε = 0.81 (2.0 mm) before becoming saturated at approximately 100 Hv.

The increasing ratio of the Vickers hardness during drawing increased with the In content. The Vickers hardness of the Cu-5.0 at.% In alloy wires increased significantly from 95 Hv to over 300 Hv after drawing to ε = 4.61 (0.3 mm). These results demonstrate that the strengthening effect achieved by drawing Cu-In alloys is significant, while the observed reduction in the conductivity of the alloys is relatively small.

Figure 11 shows representative nominal stress-strain curves obtained from the tensile test of the Cu-In alloy rods and wires after drawing to ε = 4.61 (0.3 mm). The yield (0.2% proof stress) and tensile strengths of the Cu-In alloy rods before drawing increased slightly with the In content (Fig. 4); however, the increase in the yield strength after severe drawing was significant in the Cu-In alloy wire with a higher In content, which is in good agreement with the hardening curve shown in Fig. 10. Surprisingly, the yield and tensile strengths of the Cu-5.0 at.% In alloy increased from 130 MPa and 330 MPa, respectively, to 1280 MPa and 1340 MPa, respectively, by drawing to ε = 0–4.61 (0.3 mm), while the Cu-5.0 at.% In alloy wire drawn to ε = 6.80 (0.1 mm) achieved yield and ultimate tensile strengths of 1370 MPa and 1410 MPa, respectively.

Figure 12 shows the relationship between the ultimate tensile strength and electrical conductivity of the Cu-5.0 at.% In alloy wires drawn to ε = 4.61 (0.3 mm), 5.35 (0.2 mm), and 6.80 (0.1 mm), along with that of selected conventional Cu-based alloy wires [41]. The combination of the high strength and conductivity of the Cu-5.0 at.% In alloy wires is superior to those of the conventional solid solution-strengthened Cu-based alloys, including Cu-Sn-P, Cu-Zn, and Cu-Sn alloys. This is primarily due to the ability of the In solute to efficiently reduce the SFE while avoiding a concurrent significant reduction in the conductivity. This will be discussed in greater depth in the next section. Further, the performance of the solution strengthened Cu-5.0 at.% In alloy wires drawn severely is comparable to that of existing commercial, age-hardenable Cu-Ti and Cu-Be alloy wires. The process of manufacturing the Cu-In alloy wires is far simpler than that required for extra solid solution and aging heat-treatments in age-hardenable alloys, although the high cost of indium may inhibit the widespread adoption of the process. The balance between the high strength and electrical conductivity of the Cu-In wires and the cost effectiveness of their manufacturing will be optimized in future studies by optimizing both the composition of the alloys and the deformation processing.

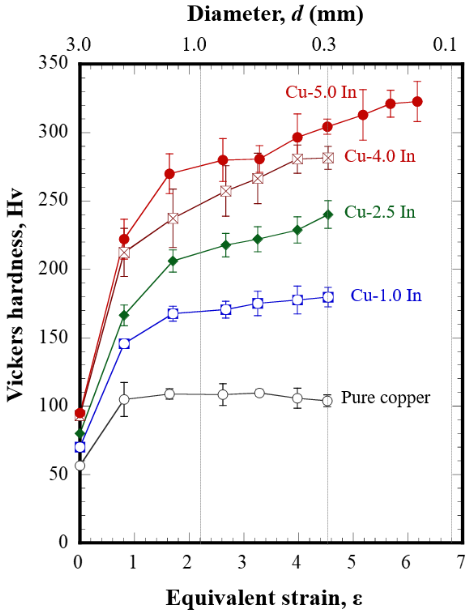

Fig. 10 Variation in the Vickers hardness of pure Cu and Cu-(1.0, 2.5, 4.0, and 5.0) at.% alloy wires as a function of equivalent strain.

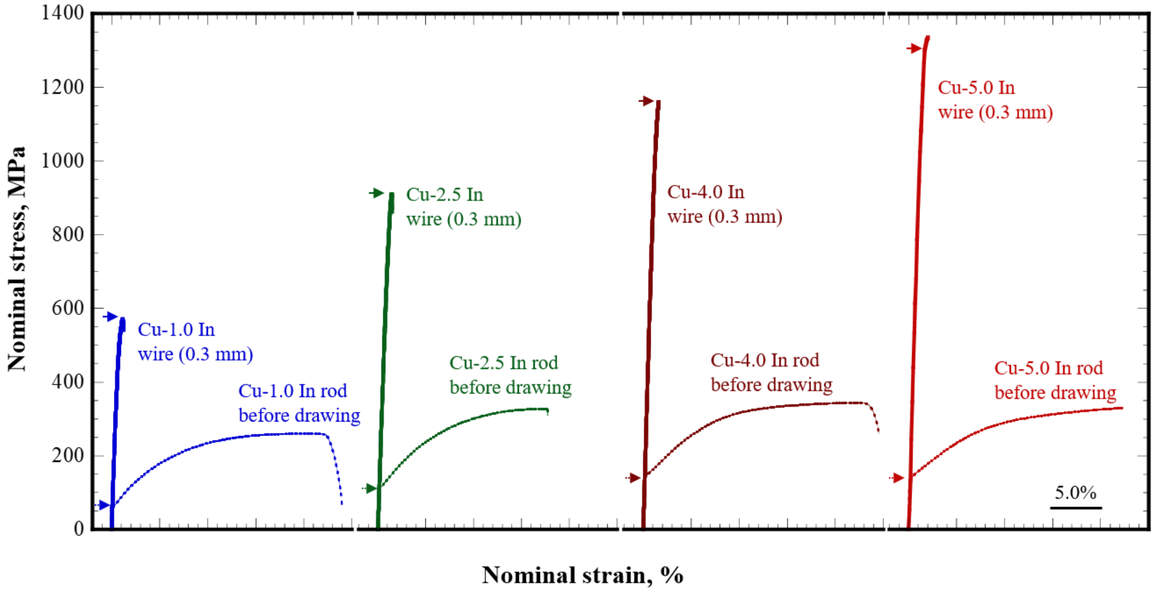

Fig. 11 Representative nominal strain–stress curves of Cu-(1.0, 2.5, 4.0, and 5.0) at.% alloy rods before drawing the wires to 0.3 mm (4.61 in equivalent strain). The arrows show the yield strength (or 0.2 % proof stress).

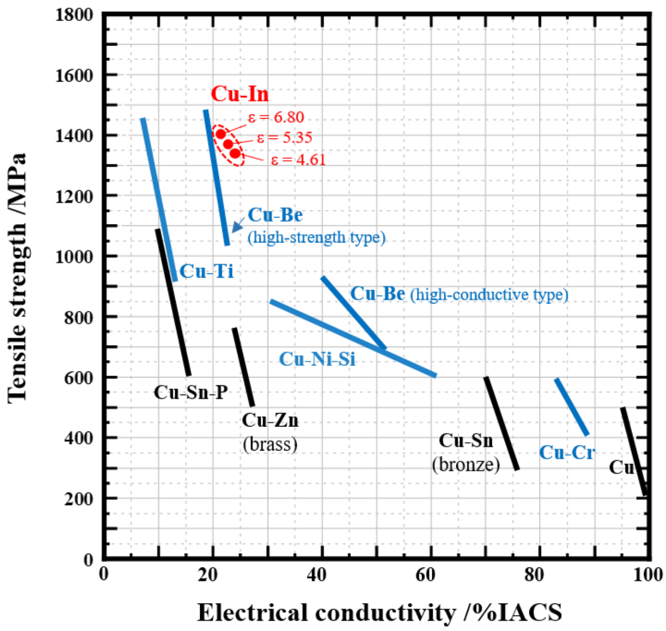

Fig. 12 Map of ultimate tensile strength and electrical conductivity of the Cu-5.0 at.% In alloy wires fabricated in this study (red) compared to those of commercial solid solution strengthened Cu-Sn-P, Cu-Zn, and Cu-Sn alloys (black), and age-hardenable Cu-Be, Cu-Ti, Cu-Ni-Si, and Cu-Cr alloys (blue) [41].

4. Discussion

The enhancement of the yield strength of Cu-5.0 at.% In alloy wires by severe drawing, $\Delta\sigma_{\mathrm{y}}$, can be modeled by the superposition of GB strengthening, $\Delta\sigma_y^{gb}$, and strain strengthening by dislocations, $\Delta\sigma_y^{dis}$, and texture effect. The texture effect is known to be small and can therefore be neglected. $\Delta\sigma_y^{gb}$ can be estimated using Hall-Petch's equation, as follows:

$$\Delta\sigma_y^{gb} = \sigma_0 + k_{\mathrm{y}} / d_g^{1/2}, \tag{3}$$

where σ_0 and k_{y} are constants independent of grain size, and d_g represents the grain size. Here, the σ_0 and k_{y} of Cu-5.0 at.% In alloys were roughly approximated as 123 MPa and 190 MPa/μm$^{1/2}$, respectively, according to the relationship between the grain size and yield strength of the Cu-5.0 at.% In alloy shown in Fig. A1 in the Appendix. A $\Delta\sigma_y^{gb}$ of 800–900 MPa was calculated from the average grain size of the Cu-5.0 at.% In alloy wire drawn to 0.3 mm (ε= 4.61), ranging from 60–80 nm (Fig. 8), using Eq. (3).

We then estimated $\Delta\sigma_y^{dis}$ from the electrical resistivity of the Cu-5.0 at.% In alloy wire (Fig. 9(b)). The increase in electrical resistivity caused by drawing is attributed to electron scattering at the GBs, and accumulated dislocations and nanotwins. The electrical resistivity of pure Cu tends to increase in proportion to $1/d_g$ (Fig. 13) [10]. Assuming that the relationship between the resistivity and gran size in pure Cu holds is the same as that in the Cu-5.0 at.% In alloy, the increase in resistivity caused by the GBs in the Cu-5.0 at.% In alloy wire is (0.8 to 1.0) × 10^{-8} Ω m (Fig. 9(b)) owing to the reduction in the grain size of the alloy from 10 μm to 60–80 nm after severe drawing. Therefore, the increase in resistivity owing to the accumulation of dislocations and nanotwins, is estimated as (0.1–0.3) ×10^{-8} Ω m.

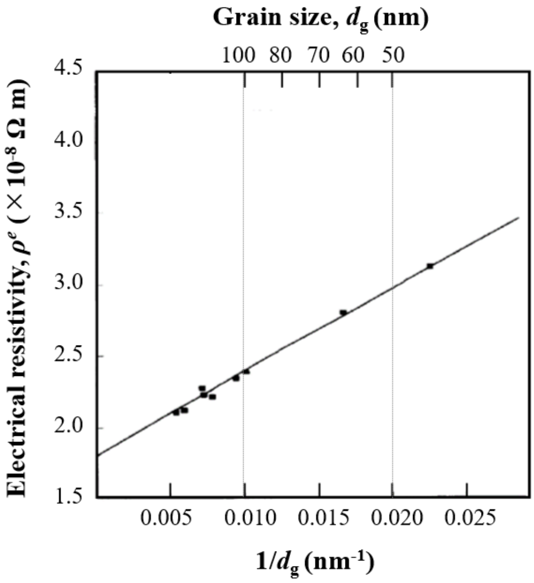

Fig. 12 Dependence of grain size on the electrical resistivity in pure Cu, which is reprinted from [10].

Because transgranular coherent nanotwins are known to have little effect on the conductivity [42], we assume that the increased resistivity of (0.1–0.3) ×10^{-8} Ω m is caused only by dislocations. Yoshinaga et al. reported that the electrical resistivity of pure Cu is proportional to the dislocation density ρ_{dis}, and the increase in the resistivity per dislocation density ρ_{dis} in pure Cu at 20 °C was approximately 2.0 × 10^{-24} Ω m^3 [11,12]. Assuming that this value is the same for the Cu-5.0 at.% In alloy, ρ_{dis} can be estimated as 3.1 × 10^{14} to 1.3 × 10^{15} m^{-2}. This value would not be abnormal, because it is similar the dislocation density observed in other severely deformed metals [43,44].

Thus, $\Delta\sigma_y^{dis}$ can be calculated from the dislocation density ρ_{dis} using Bailey-Hirsch's equation as follows:

$$\Delta\sigma_y^{dis} = M\alpha\mu b\rho_{\mathrm{dis}}^{1/2}, \qquad (4)$$

where M denotes the Taylor factor, the value of which ranges between 3.03 and 3.23 for pure Cu and Cu alloys, α is a coefficient of 0.33, μ represents the shear modulus (calculated from Young's modulus (Fig. 5) and Poisson's ratio of 0.33), and b represents Burger's vector obtained from the lattice parameter (Fig. 2). Thus, $\Delta\sigma_{dis}^{\mathrm{y}}$ was calculated to be 200–400 MPa using Eq. (4).

Considering the aforementioned estimations of $\Delta\sigma_y^{gb}$ and $\Delta\sigma_y^{dis}$, $\Delta\sigma^{\mathrm{y}}$ was calculated as 1000–1300 MPa. Here, the experimentally measured $\Delta\sigma^{\mathrm{y}}$ was 1140 MPa because the yield strength of the Cu-5.0 at.% In alloy before and after drawing was 140 MPa and 1280 MPa, respectively, as shown in Fig. 11. Thus, despite being derived from rough approximations and assumptions, the calculated and experimentally measured values are in good agreement. Therefore, the significant strengthening observed in the severely drawn Cu-5.0 at.% In alloy wire was initially caused by grain refinement and then by dislocations accumulated during drawing. The good agreement of the experimental and calculated values also suggests that the transgranular coherent nanotwins, as shown in Fig. 8(c), contributed less to strengthening during severe drawing.

The ultragrain refinement arises from the generation and bending of high-density deformation twins during drawing owing to the low SFE of the Cu-5.0 at.% In alloy. The precise SFE value of the Cu-In alloys and microstructural changes that occur during severe drawing will be the focus of future work in this area.

5. Conclusion

Cu-In alloy wires with a combination of high strength and conductivity were fabricated by casting, homogenizing, prior deformation (hot-forging and cold-grooving), heat-treatment for recovery and recrystallization, and then severe drawing. The dependence of In content in Cu solvent on the microstructural, electrical, and mechanical properties was confirmed. Further, the microstructural evolution during severe drawing and its effect on related properties were investigated. The following conclusions were drawn:

(1) The solid solution strengthening of Cu-In solid solution alloys is expected to be more effective than that of conventional binary Cu alloys owing to the large expansion of the lattice parameter. The rate at which the electrical resistivity increased with increasing In content was 0.83×10^{-8} Ω m/at.%, which is lower than that of solid solutions with other elements. The In solute in the Cu matrix significantly reduced Young's modulus, facilitating the application of these alloys in conductive springs.

(2) Cu-In alloy rods with an In content of 5.0 at.% or less could be drawn down to fine wires under an equivalent strain (ε) of 6.80. The hardness, and yield and tensile strengths of the Cu- In alloy wires increased significantly during drawing, while the conductivity gradually decreased. The Cu-5.0 at.% In alloy wire drawn to $\varepsilon = 4.61$ exhibited excellent yield and tensile strengths of 1280 MPa and 1340 MPa, respectively, with a conductivity of 24% IACS.

(3) High-density deformation twins were generated during the initial stage of drawing owing to the low SFE of the Cu-5.0 at.% In alloy. This eventually resulted in the formation of an ultrafine grain microstructure with an average grain size of 60–80 nm during the later stage of drawing to $\varepsilon = 4.61$. The significant strengthening during severe drawing was caused primarily by grain refinement and then by accumulated dislocations.

The precise nature of the SFE and twinnability of the Cu-In alloys, along with the effect of the SFE on grain refinement during severe drawing, remain to be elucidated. This investigation will form the basis of our future research in this field.

Funding sources

Funding: This work was supported by a cooperative program of Collaborative Research and Development Center for Advanced Materials (CRDAM) in IMR (No. 202112-CRKKE-0410). The authors gratefully acknowledge financial support from the Japan Society for the Promotion of Science via a Grant-in-Aid for Scientific Research (B) (No. 18H01743 and 22H01825) and from the Japan Cu and Brass Association.

Declaration of Competing Interest

The authors declare that they have no conflict of interest.

Acknowledgements

The authors thank Dr. M. Nagasako, Mr. S. Ito, and Mr. E. Aoyagi of the Institute for Materials Research (IMR) of Tohoku University for their assistance with the experiments.

References

1. X. Guoliang, W. Qiangsong, M. Xujun, X. Baiqing, P. Lijun, The precipitation behavior and strengthening of a Cu–2.0 wt% Be alloy, Mater. Sci. Eng. A 558 (2012) pp. 326–330.
2. Q. Lei, Z. Li, T. Xiao, Y. Pang, Z.Q. Xiang, W.T. Qiu, Z. Xiao, A new ultrahigh strength Cu–Ni–Si alloy, Intermetallics 42 (2013) pp. 77–84.
3. S. Semboshi, Y. Kaneno, T. Takasugi, N. Masahashi, High strength and high electrical conductivity Cu-Ti alloy wires fabricated by aging and severe drawing, Metall. Mater. Trans. A 49 (2018) pp. 4956–4965.
4. S.Z. Han, E.-A. Choi, S.H. Lim, S. Kim, J. Lee, Alloy design strategies to increase strength and its trade-offs together, Prog. Mater. Sci. 117 (2021) p. 100720.
5. S. Semboshi, R. Hariki, T. Shuto, H. Hyodo, Y. Kaneno, N. Masahsshi, Age-induced precipitating and strengthening behaviors in a Cu–Ni–Al alloy, Metall. Mater. Trans. A 52 (2021) pp. 4934–4945.
6. K. Maki, Y. Ito, H. Matsunaga, H. Mori, Solid-solution Cu alloys with high strength and high electrical conductivity, Scripta Mater. 68 (2013) pp. 777–780.
7. Y. Li, Z. Xiao, Z. Li, Z. Zhou, Z. Yang, Q. Lei, Microstructure and properties of a novel Cu‑Mg-Ca alloy with high strength and high electrical conductivity, J. Alloys Compd. 723 (2017) pp. 1162–1170.
8. N. Tsuji, T. Toyoda, Y. Minamino, Y. Koizumi, T. Yamane, M. Komatsu, M. Kiritani, Microstructural change of ultrafine-grained aluminum during high-speed plastic deformation, Mater. Sci. Eng. A 350 (2003) pp. 108–116.
9. Y. Koizumi, M. Ueyama, N. Tsuji, Y. Minamino, K. Ota, High damping capacity of ultra-fine grained aluminum produced by accumulative roll bonding, J. Alloys Compd. 30 (2003) pp. 47–51.
10. S. Riedel, J. Röber, T. Geßner, Electrical properties of Cu films produced by MOCVD.

Microelectron. Eng. 33 (1997) pp. 165–172.

11. H. Yoshinaga, Measurements of the anisotropy of the dislocation resistivity in Au, Ag, and Cu, Phys. Status Solidi 18 (1966) pp. 625–636.
12. J.W. Rutter, J. Reekie, The effect of cold working on the electrical resistivity of Cu and aluminum. Phys. Rev. 78 (1950) pp. 70–71.
13. Y.H. Zhau, X.Z, Liao, Y.T. Zhu, Z. Horita, T.G. Langdon, Influence of Stacking Fault Energy on Nanostructure Formation under High Pressure Torsion, Mater. Sci. Eng. A 410–411 (2005) pp. 188–193.
14. L. Balogh, T. Ungar, Y. Zhao, Y.T. Zhu, Z. Horita, C. Xu, T.G. Langdon, Influence of stacking-fault energy on microstructural characteristics of ultrafine-grain Cu and Cu–zinc alloys, Acta Mater. 56 (2008) pp. 809–820.
15. Y.H. Zhao, X.Z. Liao, Z. Horita, T.G. Langdon, Y.T. Zhu, Determining the optimal stacking fault energy for achieving high ductility in ultrafine-grained Cu–Zn alloys, Mater. Sci. Eng. A 15 (2008) pp. 123–129.
16. S. Qu, X.H. An, H.J. Yang, C.X. Huang, G. Yang, Q.S. Zang, Z.G. Wang, S.D. Wu, Z.F. Zhang, Microstructural evolution and mechanical properties of Cu–Al alloys subjected to equal channel angular pressing, Acta Mater. 57 (2009) pp. 1586–1601.
17. R. Kumar, S.M. Dasharath, P.C. Kang, C.C. Koch, S. Mula, Enhancement of mechanical properties of low stacking fault energy brass processed by cryorolling followed by short-annealing, Mater. Des., 67 (2015) pp. 637–643.
18. B.B. Straumal, A.R. Kilmametov, G.A. Lopez, I. Lopez-Ferreno, M.L. No, J. San Juan, H. Hahn, B. Baretzky, High-pressure torsion driven phase transformations in Cu–Al–Ni shape memory alloys, Acta Mater. 125 (2017) pp. 274–285.
19. J.O. Linde, An experimental study of the resistivity- concentration dependence of alloys. Helve. Phys. Acta 41 (1968) pp. 1007–1015.

20. H.W. King, Quantitative size-factors for metallic solid solutions, J. Mater. Sci. 1 (1966) 79–90.
21. P.C.J. Gallagher, The influence of alloying, temperature, and related effects on the stacking fault energy. Metall. Trans. 1 (1970) pp. 2429–2461.
22. Z.J. Zhang, Q.Q. Duan, X.H. An, S.D. Wu, G. Yang, Z.F. Zhang, Microstructure and mechanical properties of Cu and Cu–Zn alloys produced by equal channel angular pressing, Mater. Sci. Eng. A 528 (2011) pp. 4259–4267.
23. H. Bahmanpour, A. Kauffmann, M.S. Khoshkhoo, K.M. Youssef, S. Mula, J. Freudenberger, J. Eckert, R.O. Scattergood, C.C. Koch, Effect of stacking fault energy on deformation behavior of cryo-rolled copper and copper alloys, Mater. Sci. Eng. A 529 (2011) pp. 230–236.
24. A. Rohatgi, K.S. Vecchio, G.T. Gray III, The influence of stacking fault energy on the mechanical behavior of Cu and Cu-Al alloys: Deformation twinning, work hardening, and dynamic recovery, Metall. Mater. Trans. A 32 (2001) pp. 135–145.
25. N.M. Chavan, P. S. Phani, M. Ramakrishna, L. Venkatesh, P. Pant, G. Sundararajan, Role of stacking fault energy (SFE) on the high strain rate deformation of cold sprayed Cu and Cu–Al alloy coatings, Mater. Sci. Eng. A 814 (2021) p. 141242.
26. Z. Bahari, E. Dichi, B. Legendre, J. Dugué, The equilibrium phase diagram of the copper-indium system: A new investigation. Thermochim. Acta. 401 (2003) pp. 131–138.
27. S. Semboshi, T.J. Konno, Effect of aging in hydrogen atmosphere on electrical conductivity of Cu–3at.%Ti alloy, J. Mater. Res. 23 (2008) pp. 473–477.
28. Metals Data book, 4th edition, edited by The Jpn. Inst. Metals and Mater., publisher: Maruzen Corporation, (2017) pp. 43 (Japanese).
29. H.W. King, Quantitative size-factors for metallic solid solutions. J. Mater. Sci. 1 (1966) pp. 79–90.
30. T.H. Davis, J.A. Rayne, Specific heat and residual resistivity of binary and ternary noble-metal alloys, Phys. Rev. B 6 (1972) pp. 2931–2942.

31. J. Miyake, M.E. Fine, Electrical conductivity versus strength in a precipitated alloy, Acta Metall. Mater. 40 (1992) pp. 733–741.
32. S. Semboshi, T.J. Konno, Effect of aging in hydrogen atmosphere on electrical conductivity of Cu-3 at.% Ti alloy, J. Mater. Res. 23 (2008) pp. 473–477.
33. K. Nakanishi, H. Suzuki, Analysis of the grain size dependance on the yield stress in copper-aluminum and copper-nickel alloys, Trans JIM, 15 (1974) pp. 435–440.
34. L. Cizek, P. Kratochochvil, B. Smola, Solid solution hardening of copper crystals, J. Mater. Sci. 9 (1974) pp. 1517–1520.
35. A. Studies, P.O. Box, P.H. Uk, Review solid-solution hardening, J. Mater. Sci. 28 (1993) pp. 2557–2576.
36. K.A. Weidenmann, R. Tavangar, L. Weber, Mechanical behaviour of diamond reinforced metals, Mater. Sci. Eng. A 523 (2009) pp. 226–234.
37. N. Khobragade, K. Sikdar, B. Kumar, S. Bera, D. Roy, Mechanical and electrical properties of copper-graphene nanocomposite fabricated by high pressure torsion, J. Alloys Compd. Pp. 776 (2019) 123–132.
38. Y.B. Wang, X.Z. Liao, Y.H. Zhao, E.J. Lavernia, S.P. Ringer, Z. Horita, T.G. Langdone, Y.T. Zhu, The role of stacking faults and twin boundaries in grain refinement of a Cu–Zn alloy processed by high-pressure torsion, Mater. Sci. Eng. A 527 (2010) pp. 4959–4966.
39. C.J. Barr, K. Xia, Grain refinement in low SFE and particle-containing nickel aluminum bronze during severe plastic deformation at elevated temperatures, J. Mater. Sci. Tech. 82 (2021) pp. 57–68.
40. C.X. Huang, W. Hu, G. Yang, Z.F. Zhang, S.D. Wu, Q.Y. Wang, G. G Gottstein, The effect of stacking fault energy on equilibrium grain size and tensile properties of nanostructured copper and copper-aluminum alloys processed by equal channel angular pressing, Mater. Sci. Eng. A, 556 (2012) pp. 638–647.

41. S. Semboshi, Y. Kaneno, T. Takasugi, S.Z. Han, N. Masahashi, Effect of composition on the strength and electrical conductivity of Cu-Ti binary alloy wires fabricated by aging and intense drawing, Metall. Mater. Trans. A 50 (2019) pp. 1389–1396.
42. L. Lu, Y.F. Shen, X. Chen, L. Qian, K. Lu, Ultrahigh strength and high electrical conductivity in copper, Science, 304 (2004) pp. 422–426.
43. Y. Miyajima, S. Okubo, H. Abe, H. Okumura, T. Fujii, S. Onaka, M. Kato, Dislocation density of pure copper processed by accumulative roll bonding and equal-channel angular pressing, Mater. Charact. 104 (2015) pp. 101–106.
44. C. Wang, F. Li, L. Wei, Y. Yang, J. Dong, Experimental microindentation of pure copper subjected to severe plastic deformation by combined tension-torsion, Mater. Sci. Eng. A 571 (2013) pp. 95–102.
45. Y.Z. Tian, Y.P. Ren, S. Gao, R.X. Zheng, J.H. Wang, H.C. Pan, Z.F. Zhang, N. Tsuji, G.W. Qin, Two-stage Hall-Petch relationship in Cu with recrystallized structure, J. Mater. Sci. Tech. 48 (2020) pp. 31–35.

Appendix: Hall-Petch relationship for Cu-5.0 at.% In alloy

We surveyed the relationship between the grain size and yield strength of the Cu-5.0 at.% In alloy with a single Cu solid solution (Cu_{ss}) phase. The Cu-5.0 at.% In alloys were groove-rolled to a rod shape (with a 3.0 mm diameter) and heat-treated within a Cu_{ss} single-phase region at 500 °C for 1 min and 10 min, at 600 °C for 10 min, and at 700 °C for 10 min to obtain Cu_{ss} single phase alloys with equiaxed grain microstructures with equivalent diameters of 7 μm, 8 μm, 20 μm, and 100 μm. Figure A-1 shows the relationship between the grain size and yield strength of the Cu-5.0 at.% In alloy, together with that of pure Cu [45]. From the yield strength plots of the Cu-5.0 at.% In alloy, $\Delta\sigma^{y}_{gb}$ can be approximated using equation (A-1):

$$\Delta\sigma^{y}_{gb} = 123 + 190 / d_g^{1/2}, \qquad \text{(A-1)}$$

where $\Delta\sigma^{y}_{gb}$ denotes the increase in the yield strength caused by the GBs, and d_g represents the grain size.

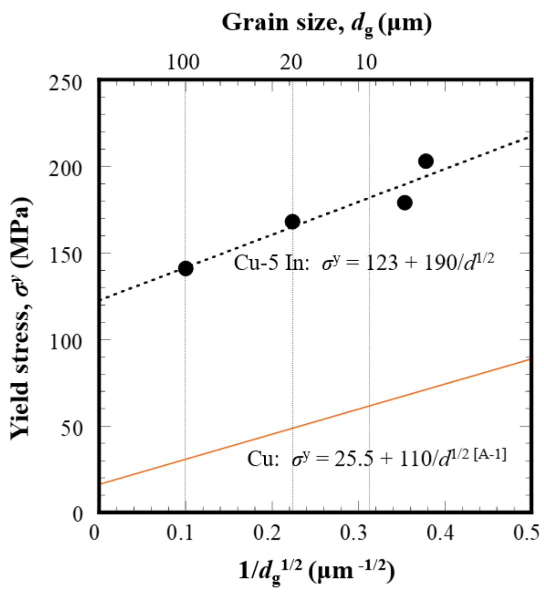

Fig. A-1 Relationship between grain size and yield strength in Cu-5.0 at.% In alloy, together with that in pure Cu.